EPJ Web of Conferences **262**, 01004 (2022) https://doi.org/10.1051/epjconf/202226201004
EXA2021

Recent progress of laser spectroscopy measurements of pionic helium

Masaki Hori[1,2,*], *Hossein* Aghai-Khozani[1,**], *Anna* Sótér[1,***], *Andreas* Dax[3], and *Dániel* Barna[4,****]

[1]Max-Planck-Institut für Quantenoptik, Hans-Kopfermann-Strasse 1, D-85748 Garching, Germany
[2]Fakultät für Physik, Ludwig-Maximilians-Universität München, 80799 Munich, Germany
[3]Paul Scherrer Institut, Forschungsstrasse 111, CH-5232 Villigen, Switzerland
[4]CERN CH-1211, Geneva 23, Switzerland

Abstract. We review the results of recent laser spectroscopy experiments on metastable pionic helium atoms at the Paul Scherrer Institute's 590 MeV cyclotron facility that was carried out by the PiHe collaboration. Some future perspectives are briefly discussed.

1 Introduction

Metastable pionic helium atoms ($\pi^4\mathrm{He}^+ \equiv \pi^- + {}^4\mathrm{He}^{2+} + e^-$) [1–5] consist of a helium nucleus, an electron in the ground state, and a negatively-charged pion in a state with high principal and orbital angular momentum quantum numbers $n \approx \ell + 1 \approx 16$. Atoms populating such states possess nanosecond-scale lifetimes against π^- nuclear absorption because the pionic orbitals have very small overlap with the helium nucleus. The deexcitation rates of the atom via electromagnetic cascade processes such as Auger and radiative decays are thus highly reduced. The long lifetime recently enabled laser spectroscopy [6, 7] of an infrared transition of $\pi^4\mathrm{He}^+$ to be carried out. This constituted the first laser spectroscopy measurement of a mesonic atom, and showed the existence of this three-body variant of pionic helium. The π^- mass [8–10] can in principle be determined with a high precision by comparing the atomic transition frequencies with the results of quantum electrodynamics (QED) calculations, as has been done for three-body antiprotonic helium ($\overline{p}\mathrm{He}^+ \equiv \overline{p} + \mathrm{He}^{2+} + e^-$) atoms [11–24]. The π^- mass can then be used to help set improved upper limits on constraints on the muon antineutrino mass by laboratory experiments [25]. Some upper limits may also be set on any exotic force [26–31] that involves the π^-. The atomic structure of $\pi^4\mathrm{He}^+$ has no hyperfine structure that arises from the spin-spin interaction between the spin-0 π^- and ^{4}He nucleus [32, 33], and so is interesting from the point of view of studying the bound-state QED of spin-0 systems. Several past experiments [34–38] based on either bubble chambers or particle counters have indirectly inferred the existence of $\pi^4\mathrm{He}^+$ atoms by observing that some π^- coming to rest in helium targets have an anomalously long lifetime. Quantitative comparisons

*e-mail: Masaki.Hori@cern.ch
**Present address: McKinsey and Company, Sophienstrasse 26, 80333 Munich, Germany
***Present address: ETH Zürich, IPA, Otto-Stern-Weg 5, 8093 Zurich, Switzerland
****Present address: Institute for Particle and Nuclear Physics, Wigner Research Centre for Physics, H-1525 Budapest 114, P.O.B. 49, Hungary

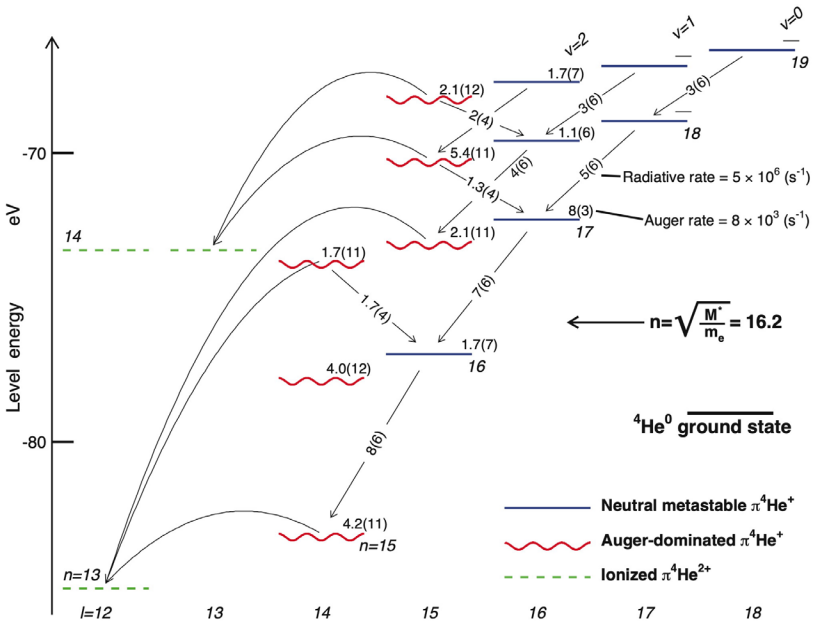

Figure 1. Energy level diagram of $\pi^4\mathrm{He}^+$. The theoretical absolute energies of the states (n, ℓ) are plotted relative to the three-body-breakup threshold. The wavy lines indicate Auger-dominated states with picosecond-scale lifetimes, the solid lines metastable states with $>$ 10 ns lifetimes. The Auger decay rates of each state are shown in s^{-1}. The dashed lines correspond to $\pi^4\mathrm{He}^{2+}$ ionic states that are formed after Auger emission. The curved arrows show the Auger transitions that have minimum $|\Delta\ell_A|$. The radiative transitions $(n, \ell) \rightarrow (n-1, \ell-1)$ and $(n, \ell) \rightarrow (n-1, \ell+1)$ are indicated by straight arrows, with the corresponding decay rates in s^{-1}. From Ref. [7].

of the experimental data with the theoretical calculations have been difficult, however, as some sets of calculated $\pi^4\mathrm{He}^+$ decay rates have differed from each other by 1–2 orders of magnitude [2, 7, 39].

2 Experimental method

The recent experiment utilized the πE5 beamline of the Paul Scherrer Institute's 590 MeV ring cyclotron facility that provided a π^- beam that had a momentum between $P = 83$ and 87 MeV/c, and an average intensity of $N_\pi = (2-3) \times 10^7$ s^{-1}. Infrared sub-nanosecond laser pulses excited a transition from a pionic state $(n, \ell) = (17, 16)$ of the neutral atom that had a nanosecond-scale lifetime, to another state $(17, 15)$ that had a lifetime of $\tau \approx 5$ ps against Auger decay [7] (see energy level diagram of Fig. 1). A two-body pionic helium ion ($\pi^4\mathrm{He}^{2+} \equiv \pi^- + \mathrm{He}^{2+}$) was formed after Auger emission of the remaining 1s electron. Atomic collisions in the experimental target caused Stark mixing between the Rydberg ionic states and the states with low ℓ values [40] as well as other possible cascade effects [41] that eventually lead to the absorption of the π^- by the helium nucleus. The high-precision laser spectroscopic study of this ion would also be interesting [42]. This allowed the resonance condition between the laser and the $\pi^4\mathrm{He}^+$ atom to be detected as a sharp peak in the rates of neutrons, protons, and deuterons that emerged from the nuclear absorption. The experiment involved numerous backgrounds of much higher intensity than the laser resonance signal.

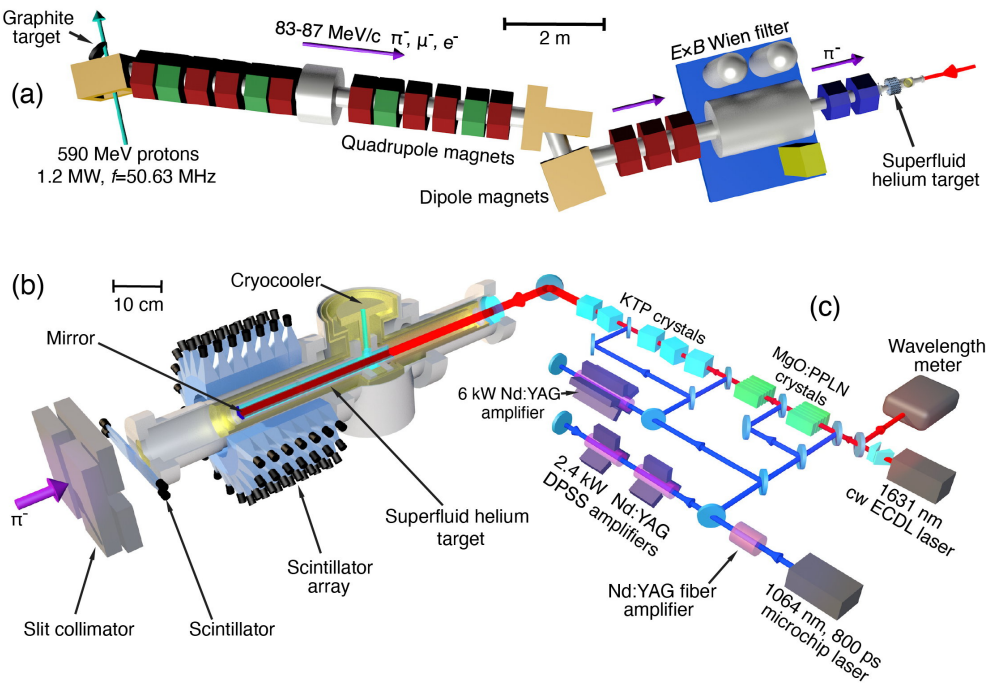

Figure 2. (a): Schematic layout of the πE5 experimental beamline showing the positions of the Wien filter and superfluid helium target. (b): Layout of the experimental target. (c) Schematic of the laser system, see text. From Ref. [6].

The measurement therefore required detectors of 1 ns-scale timing resolution and moderate energy resolution to isolate the signal.

A Wien filter was placed in the beamline upstream of the experiment and used to divert most of the contaminant e^- that arrived at a rate $> 3 \times 10^9$ s^{-1} into the blades of a collimator. The remaining π^- beam was focused into a superfluid helium target. The beam first passed through a segmented plastic scintillator plate with a thickness $t_d = 4.7$ mm. The π^- arrived at the experimental target at timings spaced by regular intervals $\Delta t = 19.75$ ns, which arose from the $f_a = 50.63$ MHz acceleration radiofrequency (RF) of the cyclotron. Each RF cycle contained on average $N_\pi/f_a \approx 0.4 - 0.6$ pions. A $\approx 2\%$ fraction of the π^- that came to rest in the helium target (see Fig. 2 (a)) with a length of 150 mm, diameter of 42 mm, and a temperature of $T = 1.7$ K formed metastable $\pi^4\mathrm{He}^+$. A 800 ps-long laser pulse of diameter $d = 25$ mm, pulse energy $E = 10$ mJ, repetition rate $f_r = 80.1$ Hz and wavelength $\lambda \approx 1631$ nm entered the target through a pair of fused silica windows and irradiated the atoms. The estimated $\pi^4\mathrm{He}^+$ production rate of $> 3\times10^5$ s^{-1} implied a probability of coincidence of 10^{-3} for a laser pulse to irradiate a long-lived atom.

The nuclear fragments that emerged from the π^- absorption [7] with a typical kinetic energy of a few tens of MeV were measured by an array of 140 plastic scintillation counters that covered a solid angle of $\approx 2\pi$ steradians seen from the target. The size $40 \times 35 \times 34$ mm^3 of each counter was chosen to obtain a significant ($< 10\%$) detection efficiency for $E \geq 25$ MeV neutrons [7], while allowing the rejection of most of the background e^- that were produced either from μ^- decay or the particle beam. These e^- deposited an average

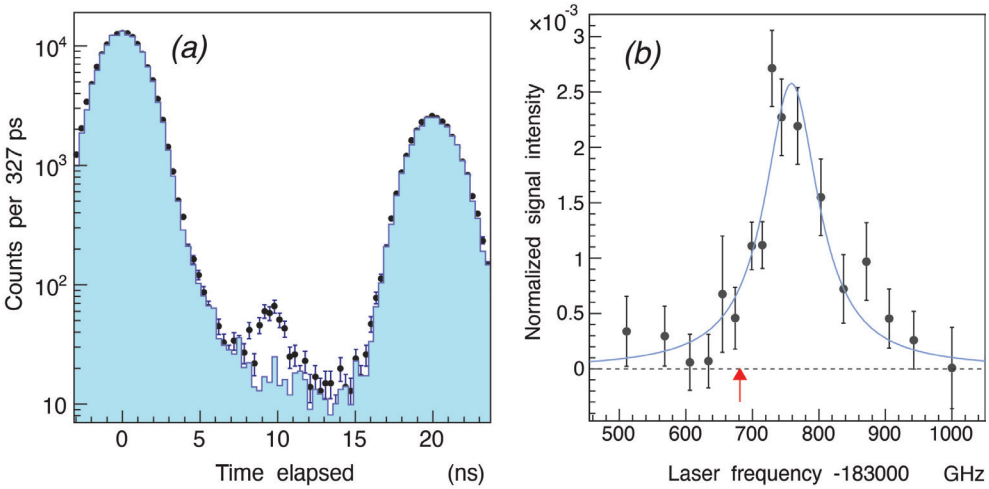

Figure 3. (a): Time spectra of nuclear fragments (mainly protons, neutrons, and deuterons) that emerged from π^- absorption in helium nuclei measured with (indicated by filled circles) and without (blue histogram) the laser irradiation of the target. The peak in the former spectrum at $t = 9$ ns shows the laser resonance signal of the transition $(n, \ell) = (17, 16) \rightarrow (17, 15)$. (b): The spectral profile of the transition as a function of the laser frequency. The red arrow indicates the position of the theoretical transition frequency, see text. From Ref. [6].

energy $\Delta E = 6 - 8$ MeV in the counters. We developed a data acquisition system based on waveform digitizers to record the signal waveforms of the 140 counters during each laser pulse arrival [43–45] at a sampling rate $f = 3.06$ Gs·s^{-1}. An earlier version of the electronics was used by the ASACUSA collaboration to determine upper limits on the cross sections of antiprotons with kinetic energy $E \approx 125$ keV annihilating in thin target foils [44, 46, 47]. The results of the experiment were compared with the annihilation cross sections measured at antiproton energies $E = 5.3$ MeV [48, 49].

The blue histogram of Fig. 3 (a) represents the time distribution of scintillator hits that were measured without laser irradiation. The π^- arrivals at $t = 0$ and 19.75 ns produced peaks in the spectrum that contained > 97% of the π^- that were immediately absorbed by the helium nuclei. The metastable atoms that decayed spontaneously with a lifetime of $\tau = (7 \pm 2)$ ns were contained in the remaining (2.1 ± 0.7)% fraction of the events in the intervals between the π^- arrivals. The shape of this experimental spectrum is in rough agreement with the results of a Monte Carlo simulation [7].

The laser pulses were produced by an injection-seeded, optical parameteric generator (indicated as OPG in Fig. 2(b)) and amplifier (OPA). The laser was precisely fired in synchronization with the RF signal of the cyclotron by pumping the OPG-OPA with a diode-pumped solid state (DPSS) neodymium-doped yttrium aluminium garnet (Nd:YAG) laser of single pass design. The seed light for the OPG-OPA was produced by a continuous-wave (cw) external-cavity diode laser (ECDL). The OPG was carried out using magnesium oxide doped periodically-polled lithium niobate (MgO:PPLN) crystals which produced laser pulses of energy $E = 70$ uJ. The beam was then amplified via OPA to $E = 10$ mJ using five potassium titanyl phosphate (KTP) crystals. The portion of the laser beam with a narrow spectral component had a linewidth of around 10 GHz. The OPG and OPA processes caused a 3 GHz uncertainty in the determination of the laser optical frequency.

3 Experimental results

We first searched for the $(n, l) = (16, 15) \rightarrow (17, 14)$ transition by irradiating the target with resonant laser pulses that were generated by a laser based on dye and Ti:sapphire [50] pulsed amplification. The laser was scanned over a 200 GHz range around the theoretical transition frequency, but no resonance was detected. Theoretical calculations [3] show that the resonance daughter state $(n, \ell) = (17, 14)$ strongly couples to an electronically excited state of $\pi^4\mathrm{He}^+$. This is expected to destabilize the daughter state during atomic collisions, as was seen in the case of $\overline{p}\mathrm{He}^+$ [51–53].

We next searched for the resonance $(16, 15) \rightarrow (16, 14)$ by tuning the laser to the theoretical transition wavelength $\lambda = 1515.3$ nm. The daughter state $(16, 14)$ is predicted to have a lifetime $\tau = 250$ fs [7] which corresponds to a large resonance width $\Gamma_A = 640$ GHz. We accumulated $> 6 \times 10^7$ detected π^- arrivals over several weeks, but no statistically significant signal was detected. The reason for this non-observation is not understood, but collisions with other helium atoms may destroy the π^- population that occupies the resonance parent state $(16, 15)$. Atomic collisions have been observed to similarly shorten the lifetimes of some $\overline{p}\mathrm{He}^+$ states [18, 19, 54–59]. Another possible reason for the non-observation may be that a negligible fraction of π^- are captured into the parent state $(16, 15)$. Some lower-n states of $\overline{p}\mathrm{He}^+$ have shown a small primary population [56, 60–64].

We then searched for the transition $(17, 16) \rightarrow (17, 15)$. The time spectrum corresponding to 2.5×10^7 π^- arrivals that was measured with the wavelength of the OPG-OPA laser tuned to $\lambda \approx 1631.4$ nm is plotted in Fig. 3(a) using filled circles with error bars. A peak containing about 300 events was observed at $t \approx 9$ ns, with a signal-to-noise ratio of 4 and a statistical significance corresponding to > 7 standard deviations. The $\Delta t = 2$ ns width of the peak is compatible with the dispersion of the time-of-flights of the fission fragments that arrived at the scintillator array. The detected rate of resonant $\pi^4\mathrm{He}^+$ events of 3 h^{-1} is roughly compatible with the production rate of $> 3 \times 10^5$ s^{-1} of the pionic atoms and with the above Monte Carlo simulations [7]. The simulation assumed that most of the metastable atoms populate the parent state $(17, 16)$. As expected, the signal decreased and disappeared when the laser was detuned off the resonance frequency.

The resonance profile shown in Fig. 3 (b) was obtained by scanning the laser frequency and plotting the number of detected events under the laser-induced peak at $t \approx 9$ ns. Each data point contains data collected over a 20–30 h period. The statistical uncertainty arising from the finite number of resonant $\pi^4\mathrm{He}^+$ events is indicated by the vertical error bars. The measured resonance width of ≈ 100 GHz is believed to arise from the 33 GHz Auger width [7] of the daughter state $(17, 15)$ predicted by theory, collisional and power broadening effects [4] which are estimated to cause a contribution of ≈ 50 GHz, and the ≈ 10 GHz linewidth of the narrowband spectral component of the OPG-OPA laser. Atomic collisions that shorten [3, 54] the lifetime of the resonance daughter state may cause an additional broadening. The interaction between the electron spin and the orbital angular momentum of π^- is expected to give rise to a pair of fine structure sublines that are spaced by a frequency interval of 3.0 GHz [7, 19]. These sublines cannot be resolved in this spectrum, since the splitting is much smaller than the natural width of the resonance. The reduced χ^2 value of the best fit (indicated by the blue curve) of two overlapping Lorentzian functions that take these fine structure sublines into account was 1.0.

The resonance centroid was determined as $\nu_{\mathrm{exp}} = 183760(6)(6)$ GHz. The statistical uncertainty due to the finite number of detected $\pi^4\mathrm{He}^+$ events is 6 GHz, whereas the systematic uncertainty of 6 GHz contains the contributions related to the selection of the fit function and the determination of the laser frequency. The experimental frequency ν_{exp} is larger than the theoretical value [7] $\nu_{\mathrm{th}} = (183681.8 \pm 0.5)$ GHz by $\Delta\nu = (78 \pm 8)$ GHz. This differ-

ence is believed to be caused by atomic collisions that shift the resonance frequency [4]. Similar shifts have previously been observed [20, 54, 58, 65] in some $\overline{p}\mathrm{He}^+$ resonances. A theoretical calculation based on the impact approximation of the binary collision theory of spectral lineshapes predicted that the gradient of this shift at a target temperature $T = 4$ K is $d\nu/d\rho = (4.4 - 6.5) \times 10^{-21}$ GHz·cm^3 [4]. The blueshift at superfluid density expected from this calculation corresponds to between $\Delta\nu = 96$ and 142 GHz, which roughly agrees with the experimental result. This shift must be experimentally measured in future experiments before the π^- mass can be precisely determined.

We plan to search for other transitions such as $(17, 16)\rightarrow(16, 15)$ that are expected to be narrower by a factor of at least 10^{-3} compared to the resonance observed in the above experiment. Helium gas targets in which the collisional shifts are small may be used, together with various laser spectroscopic techniques [14, 17, 21, 50]. The precision of the theoretical calculation of the transition frequencies is currently limited by the experimental uncertainty of the π^- mass. The precision of the QED calculations themselves [7] may be improved to a fractional precision of better than 10^{-8} for some transitions, as in the cases of HD^+ [66, 67] molecular ions and $\overline{p}\mathrm{He}^+$ [11, 12] atoms. These experiments at PSI will complement the $\overline{p}\mathrm{He}^+$ experiments carried out by the ASACUSA collaboration at the ELENA facility [68–71]. In the far future, these laser spectroscopy experiments may lead to studies of the shifts of the atomic binding energies that arise from the strong interaction [72]. Some novel methods of producing pionic atoms at the proposed gamma factory at CERN [73] may also be studied.

References

[1] G.T. Condo, Phys. Lett. **9**, 65 (1964)
[2] J.E. Russell, Phys. Rev. Lett. **23**, 63 (1969)
[3] V.I. Korobov, A.K. Bekbaev, D.T. Aznabayev, S.A. Zhaugasheva, J. Phys. B **48**, 245006 (2015)
[4] B. Obreshkov, D. Bakalov, Phys. Rev. A **93**, 062505 (2016)
[5] D. Baye, J. Dohet-Eraly, Phys. Rev. A **103**, 022823 (2021)
[6] M. Hori, H. Aghai-Khozani, A. Sótér, A. Dax, D. Barna, Nature **581**, 37 (2020)
[7] M. Hori, A. Sótér, V.I. Korobov, Phys. Rev. A **89**, 042515 (2014)
[8] S. Lenz et al., Phys. Lett. B **416**, 50 (1998)
[9] M. Trassinelli et al., Phys. Lett. B **759**, 583 (2016)
[10] M. Daum, R. Frosch, P.-R. Kettle, Phys. Lett. B **796**, 11 (2019)
[11] V.I. Korobov, L. Hilico, J.-P. Karr, Phys. Rev. Lett. **112**, 103003 (2014)
[12] V. Korobov, L. Hilico, J.-P. Karr, Phys. Rev. A **89**, 032511 (2014)
[13] V.I. Korobov, Phys. Rev. A **89**, 014501 (2014)
[14] M. Hori et al., Phys. Rev. Lett. **96**, 243401 (2006)
[15] T. Pask et al., J. Phys. B **41**, 081008 (2008)
[16] S. Friedreich et al., Phys. Lett. B **700**, 1 (2011)
[17] M. Hori et al., Nature **475**, 484 (2011)
[18] T. Kobayashi et al., J. Phys. B **46**, 245004 (2013)
[19] S. Friedreich et al., J. Phys. B **46**, 125003 (2013)
[20] A. Adamczak, D. Bakalov, Phys. Rev. A **88**, 042505 (2013)
[21] M. Hori et al., Science **354**, 610 (2016)
[22] M.H. Hu, S.M. Yao, Y. Wang, W. Li, Y.Y. Gu, Z.X. Zhong, Chem. Phys. Lett. **654**, 114 (2016)
[23] D. Baye, J. Dohet-Eraly, P. Schoofs, Phys. Rev. A **99**, 022508 (2019)

[24] Z.D. Bai, Z.X. Zhong, Z.C. Yan, T.Y. Shi, Chin. Phys. B **30**, 023101 (2021)
[25] K. Assamagan et al., Phys. Rev. D **53**, 6065 (1996)
[26] E. Salumbides, W. Ubachs, V.I. Korobov, J. Mol. Spectrosc. **300**, 65 (2014)
[27] J. Murata, S. Tanaka, Class. Quantum Gravity **32**, 033001 (2015)
[28] F. Ficek et al., Phys. Rev. Lett. **120**, 183002 (2018)
[29] A.S. Lemos, G.C. Luna, E. Maciel, F. Dahia, Class. Quantum Gravity **36**, 245021 (2019)
[30] M. Germann et al., Phys. Rev. Research **3**, L022028 (2021)
[31] H. Banks, M. McCullough, Phys. Rev. D **103**, 075018 (2021)
[32] J. Koch, F. Scheck, Nucl. Phys. A **340**, 221 (1980)
[33] M. Trassinelli, P. Indelicato, Phys. Rev. A **76**, 012510 (2007)
[34] J.G. Fetkovich, E.G. Pewitt, Phys. Rev. Lett. **11**, 290 (1963)
[35] M.M. Block et al., Phys. Rev. Lett. **11**, 301 (1963)
[36] M.M. Block, J.B. Kopelman, C.R. Sun, Phys. Rev. **140**, B143 (1965)
[37] O.A. Zaimidoroga, R.M. Sulyaev, V.M. Tsupko-Sitnikov, Sov. Phys. JETP **25**, 63 (1967)
[38] S.N. Nakamura et al., Phys. Rev. A **45**, 6202 (1992)
[39] J.E. Russell, Phys. Rev. A **1**, 742 (1970)
[40] M. Hori et al., Phys. Rev. Lett. **94**, 063401 (2005)
[41] G.Y. Korenman, S.N. Yudin, Eur. Phys. J. D **75**, 64 (2021)
[42] J. Zatorski, K. Pachucki, Phys. Rev. A **82**, 052520 (2010)
[43] A. Sótér et al., Rev. Sci. Instrum. **85**, 023302 (2014)
[44] K. Todoroki et al., Nucl. Instr. and Meth. A **835**, 110 (2016)
[45] Y. Murakami, H. Aghai-Khozani, M. Hori, Nucl. Instrum. and Meth. A **933**, 75 (2019)
[46] H. Aghai-Khozani et al., Eur. Phys. J. Plus **127**, 125 (2012)
[47] H. Aghai-Khozani et al., Nucl. Phys. A **1009**, 122170 (2021)
[48] A. Bianconi et al., Phys. Lett. B **704**, 461 (2011)
[49] H. Aghai-Khozani et al., Nucl. Phys. A **970**, 366 (2018)
[50] M. Hori, A. Dax, Opt. Lett. **34**, 1273 (2009)
[51] H. Yamaguchi et al., Phys. Rev. A **66**, 022504 (2002)
[52] H. Yamaguchi et al., Phys. Rev. A **70**, 012501 (2004)
[53] O.I. Kartavtsev, D.E. Monakhov, S.I. Fedotov, Phys. Rev. A **61**, 062507 (2000)
[54] M. Hori et al., Phys. Rev. Lett. **87**, 093401 (2001)
[55] M. Hori et al., Phys. Rev. Lett. **91**, 123401 (2003)
[56] M. Hori et al., Phys. Rev. A **70**, 012504 (2004)
[57] B.D. Obreshkov, D.D. Bakalov, B. Lepetit, K. Szalewicz, Phys. Rev. A **69**, 042701 (2004)
[58] A. Sótér et al., to be published (2022)
[59] V.I. Korobov, Z.X. Zhong, Q.L. Tian, Phys. Rev. A **92**, 052517 (2015)
[60] M. Hori et al., Phys. Rev. Lett. **89**, 093401 (2002)
[61] J.S. Cohen, Rep. Prog. Phys. **67**, 1769 (2004)
[62] K. Tőkési, B. Juhász, J. Burgdörfer, J. Phys. B **38**, S401 (2005)
[63] X.M. Tong, K. Hino, N. Toshima, Phys. Rev. Lett. **101**, 163201 (2008)
[64] K. Sakimoto, Phys. Rev. A **91**, 042502 (2015)
[65] D. Bakalov, B. Jeziorski, T. Korona, K. Szalewicz, E. Tchoukova, Phys. Rev. Lett. **84**, 2350 (2000)
[66] S. Alighanbari, G.S. Giri, F.L. Constantin, V.I. Korobov, S. Schiller, Nature **581**, 152 (2020)

[67] S. Patra et al., Science **369**, 1238 (2020)
[68] V. Chohan et al., CERN-2014-002, Geneva, Switzerland (2014)
[69] D. Gamba et al., *ELENA COMMISSIONING*, in *Proceedings of North American Particle Accelerator Conference NAPAC2019, Lansing MI, USA* (2019), p. WEYBB1
[70] M. Hori, J. Walz, Prog. Part. Nucl. Phys. **72**, 206 (2013)
[71] M. Hori, V.I. Korobov, Phys. Rev. A **81**, 062508 (2010)
[72] A. Hirtl et al., Eur. Phys. J. A **57**, 70 (2021)
[73] V.V. Flambaum, J. Jin, D. Budker, Phys. Rev. C **103**, 054603 (2021)